Atmospheric Chemistry of Perfluoroaldehydes (C x F 2 x +1 CHO) and Fluorotelomer Aldehydes (C x F 2 x +1 CH 2 CHO): Quantification of the Important Role of Photolysis

ARTICLE *in* THE JOURNAL OF PHYSICAL CHEMISTRY A · NOVEMBER 2006

Impact Factor: 2.69 · DOI: 10.1021/jp064262k · Source: PubMed

9 AUTHORS, INCLUDING:

Malisa S. Chiappero
National Scientific and Technical Research C…
17 PUBLICATIONS **88** CITATIONS
SEE PROFILE

Robert L Waterland
Dupont
32 PUBLICATIONS **640** CITATIONS
SEE PROFILE

Robert C Buck
The Chemours Company
86 PUBLICATIONS **3,569** CITATIONS
SEE PROFILE

Atmospheric Chemistry of Perfluoroaldehydes ($C_xF_{2x+1}CHO$) and Fluorotelomer Aldehydes ($C_xF_{2x+1}CH_2CHO$): Quantification of the Important Role of Photolysis

Malisa S. Chiappero,[†] Fabio E. Malanca,[†] Gustavo A. Argüello,*[,†] Steven T. Wooldridge,[‡] Michael D. Hurley,[‡] James C. Ball,[‡] Timothy J. Wallington,*[,‡] Robert L. Waterland,[§] and Robert C. Buck[§]

INFIQC, Departamento de Físico Química, Facultad de Ciencias Químicas, Universidad Nacional de Córdoba, Ciudad Universitaria, 5000 Córdoba, Argentina, Ford Research Laboratory, SRL-3083, Ford Motor Company, Dearborn, Michigan 48121-2053, and E. I. du Pont de Nemours and Company, Incorporated, 1007 Market Street, Wilmington, Delaware 19898

Received: July 6, 2006; In Final Form: August 22, 2006

The UV absorption spectra of CF_3CHO, C_2F_5CHO, C_3F_7CHO, C_4F_9CHO, CF_3CH_2CHO, and $C_6F_{13}CH_2CHO$ were recorded over the range 225−400 nm at 249−297 K. $C_xF_{2x+1}CHO$ and $C_xF_{2x+1}CH_2CHO$ have broad absorption features centered at 300−310 and 290−300 nm, respectively. The strength of the absorption increases with the size of the C_xF_{2x+1} group. There was no discernible (<5%) effect of temperature on the UV spectra. Quantum yields for photolysis at 254 and 308 nm were measured. Quantum yields at 254 nm were 0.79 ± 0.09 (CF_3CHO), 0.81 ± 0.09 (C_2F_5CHO), 0.63 ± 0.09 (C_3F_7CHO), 0.60 ± 0.09 (C_4F_9CHO), 0.74 ± 0.08 (CF_3CH_2CHO), and 0.55 ± 0.09 ($C_6F_{13}CH_2CHO$). Quantum yields at 308 nm were 0.17 ± 0.03 (CF_3CHO), 0.08 ± 0.02 (C_4F_9CHO), and 0.04 ± 0.01 (CF_3CH_2CHO). The quantum yields decrease with increasing size of the C_xF_{2x+1} group and with increasing wavelength of the photolysis light. The photolysis quantum yield at 308 nm for CF_3CHO measured here is a factor of at least 8 greater than that reported previously. Photolysis is probably the dominant atmospheric fate of $C_xF_{2x+1}CHO$ ($x = 1-4$) and is an important fate of $C_xF_{2x+1}CH_2CHO$ ($x = 1$ and 6). These results have important ramifications concerning the yield of perfluorocarboxylic acids in the atmospheric oxidation of fluorotelomer alcohols.

1. Introduction

Perfluoroalkyl sulfonate (PFAS) and carboxylate (PFCA) surfactants are highly stable species which have been found globally in the environment.[1−4] Potential sources of these substances include their direct manufacture and use as well as indirect production via atmospheric oxidation of volatile precursors.[5,6] Several potential PFCA precursors such as perfluoroalkyl sulfonamides ($F(CF_2)nSO_2N(R)(R')$; R = H, Me, Et; R′ = H, $-CH_2CH_2OH$; $n = 4-8$) and fluorotelomer alcohols (FTOHs; $C_nF_{2n+1}CH_2CH_2OH$; $n = 2$, 4, 6) have been identified in air,[7−10] and smog chamber and biodegradation studies indicate that they can degrade in the environment to form PFCAs.[11−15] The partitioning properties of these substances which dictate their atmospheric gas-phase availability versus removal have only recently been investigated.[16,17]

Other than for trifluoroacetic acid (TFA),[18] no natural source of PFCAs has been proposed. Two explanations for the ubiquity of PFCAs in biota in remote regions have been advanced: first, the presence of widely distributed precursor compounds (presumably of anthropogenic origin) in the atmosphere that degrade to give PFCAs; second, transport of PFCAs by (i) rivers from industrial areas to the ocean, (ii) ocean currents to remote locations, and (iii) sea salt aerosol to remote inland locations.

Atmospheric oxidation of $C_nF_{2n+1}CH_2CH_2OH$ proceeds via the formation of fluorotelomer aldehydes ($C_nF_{2n+1}CH_2CHO$) and perfluoraldehydes ($C_nF_{2n+1}CHO$). Atmospheric chemistry involving $C_nF_{2n+1}CHO$ has been suggested as a source of PFCAs.[19] The atmospheric fate of fluorotelomer aldehydes and perfluoraldehydes is of critical importance in determining the atmospheric oxidation of FTOHs, which involve photolysis, reaction with OH radicals and water. However, the relative importance of these processes is unclear.

There are relatively few data available concerning the atmospheric photolysis of fluorinated aldehydes.[20,21] In one of the few studies in this area, Sellevåg et al.[21] report that over the wavelength range 290−400 nm the effective quantum yields for photolysis of CF_3CHO and CF_3CH_2CHO are <0.02 and <0.04, respectively. This finding is both interesting and important. It is interesting because it suggests that the behavior of these fluorinated aldehydes is very different from their nonfluorinated counterparts which readily undergo photolysis. It is important because it implies lower limits for tropospheric lifetimes with respect to photolysis, which render this loss process of relatively minor atmospheric importance.

The temperature in the atmosphere varies with altitude. For an accurate description of the atmospheric fate of fluorinated aldehydes, it is desirable to have UV spectra recorded over a range of atmospherically relevant temperatures (as has been reported for molecules derived from the decomposition of CFCs,[22] HCHO,[23] and peroxynitrates[24,25]). No such data are available currently.

The present work was conducted to improve our understanding of the atmospheric fate of fluorinated aldehydes. The work

* Corresponding authors. E-mail addresses: gaac@fisquim.fcq.unc.edu.ar, twalling@ford.com.
[†] Universidad Nacional de Córdoba.
[‡] Ford Motor Company.
[§] E. I. du Pont de Nemours and Co., Inc.

10.1021/jp064262k CCC: $33.50
Published on Web 10/07/2006

had four goals: first, to extend the database of UV spectra of fluorinated aldehydes; second, to quantify the effect of temperature on the UV spectra of fluorinated aldehydes; third, to investigate the quantum yields for photolysis of fluorinated aldehydes at wavelengths relevant for tropospheric chemistry; fourth, to estimate the likely importance of photolysis as an atmospheric loss for fluorinated aldehydes. Experiments were performed employing low-pressure Hg arc and excimer laser UV light sources. FTIR spectroscopy was used to monitor the concentration of the fluorinated aldehydes. Results are discussed with respect to the literature data and atmospheric fate of fluorinated aldehydes.

2. Experimental Section

Gas samples were manipulated using conventional greaseless high-vacuum systems. Pressures were measured using capacitance manometers. Samples were expanded into evacuated cells connected to the vacuum lines. The aldehydes were purchased (typically as hydrates) from commercial sources: Aldrich Chemical Co., Synquest Laboratories, or P&M-Invest Ltd. The aldehydes were liberated from the hydrates by reacting with P_2O_5.[26] All reactants were subjected to freeze−pump−thaw cycling before use. Sample purities were checked using FTIR spectroscopy; there were no observable impurities. Straight-chain isomers *n*-C_3F_7CHO, *n*-C_4F_9CHO, and *n*-$C_6F_{13}CH_2CHO$ were studied in the present work. For simplicity, we will refer to these species as C_3F_7CHO, C_4F_9CHO, and $C_6F_{13}CH_2CHO$ in the rest of this article. Unless otherwise stated, all quoted uncertainties are 2 standard deviations from regression analyses.

2.1. Quantum Yield Measurements. Two different experimental systems were used to measure quantum yields. Experiments employing photolysis at 254 nm were performed using a quartz cell with an optical path of 23 cm fitted with KBr windows that allowed simultaneous IR measurements and photolysis with a low-pressure mercury lamp (OSRAM, 10 W). A Bruker IFS 28 FTIR was used to follow aldehyde loss and product formation. The spectral resolution was 2 cm^{-1}, and four scans were typically co-added to acquire the IR spectra. The 30 s time required to record and average four interferograms was short compared to the 5−100 min UV irradiation times used in the present work.

Experiments employing 308 nm photolysis were performed using a 17.75 cm optical path Pyrex cell (4.4 cm diameter, 270 cm^3 volume) fitted with KBr windows that was placed in the optical path of a 308 nm XeCl excimer laser. The beam profile was approximately 2.5 × 1.1 cm and was positioned to traverse the middle of the cell. The laser power was operated at a power of 100 mJ $pulse^{-1}$. Control experiments established that after passing through the empty cell the power was reduced to approximately 40 mJ $pulse^{-1}$ by absorption, scattering, and reflection by the cell windows. The cell and windows were approximately 10 years old, and a slight clouding of the KBr windows was evident, which probably accounts for the observed decrease in energy. Under the assumption that both windows have equal effect, the power of the laser pulses within the cell is estimated to be approximately 70 mJ $pulse^{-1}$. After the cell had been exposed to the desired number of laser pulses, it was placed in the sample compartment of a Mattson Sirus 100 FTIR spectrometer. IR analysis was used to monitor the loss of the aldehyde using a spectral resolution of 0.25 cm^{-1} with 32 scans co-added to obtain the IR spectra.

In both sets of experiments, a reference chemical actinometer was employed. For experiments at 254 nm, perfluoroacetic anhydride ($\sigma = (2.28 \pm 0.03) \times 10^{-19}$ cm^2 $molecule^{-1}$, $\phi = 0.29 \pm 0.02$)[27] was employed as the reference. For experiments at 308 nm, acetaldehyde ($\sigma = 3.33 \times 10^{-20}$ molecule cm^2, $\phi = 0.332$)[28] was employed. All measurements were performed in the presence of excess NO to scavenge the radicals formed in the photolysis and ensure that they do not contribute to secondary loss of the aldehydes.

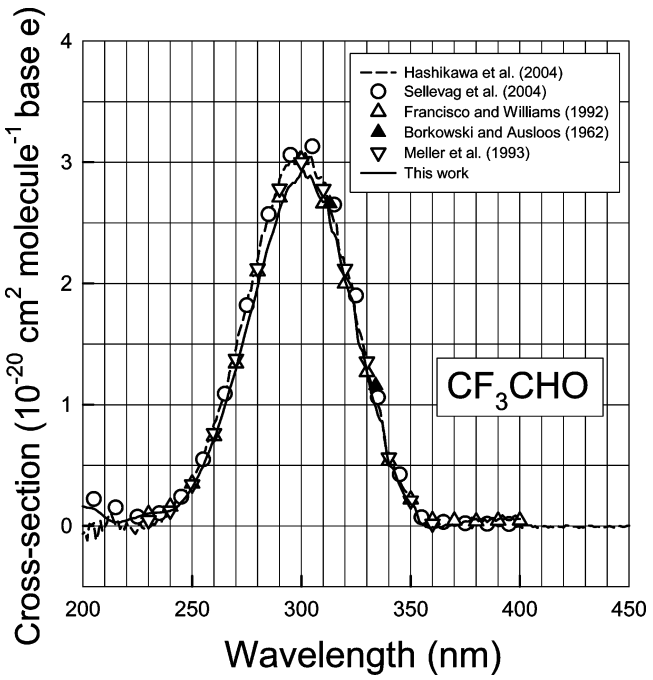

Figure 1. UV absorption cross sections for CF_3CHO from Borkowski and Ausloos[29] (filled triangles), Francisco and Williams[31] (triangles), Meller et al.[32] (inverted triangles), Sellevåg et al. (circles),[21] Hashikawa et al.[33] (dashed line), and the present work (solid line).

2.2. Low-Temperature UV Spectra. The experimental setup used to acquire the low-temperature spectra is described elsewhere[24] and is described only briefly here. A 10 cm quartz cell wrapped with cooling coils was placed inside a metal compartment with two quartz windows. The compartment could be evacuated providing thermal isolation of the quartz cell while allowing transmission of UV light. The whole device was placed in the optical path of an Agilent diode array 4853 UV spectrometer operated at 1 nm resolution. Spectra were recorded using 1.5−20 mbar of sample in the absence of added diluent gas. The temperatures were regulated, using a cryostat, between 298 and 249 K to within 1 °C. The maximum pressures of the aldehydes were adjusted to avoid condensation of liquid aldehyde at low temperatures. Absorption spectra were first measured with the sample at room temperature. The temperature was then reduced, and spectra were acquired at 281, 265, and 249 K. The cell was then warmed to room temperature, and spectra were recorded at 265 and 281 K to check the experimental reproducibility. This process was repeated using different partial pressures of sample to check the linearity of absorption with concentration. $C_6F_{13}CH_2CHO$ has a relatively low vapor pressure, and it was not possible to record spectra for this compound at subambient temperature. A single 1.5 mbar sample was used to record the room-temperature UV spectrum of this compound.

3. Results

3.1. UV Absorption Spectra at 297 K. UV absorption spectra of CF_3CHO, C_2F_5CHO, C_3F_7CHO, C_4F_9CHO, CF_3CH_2CHO, and $C_6F_{13}CH_2CHO$ at 297 K are shown in Figures 1−6. The insets in Figures 3−5 show the linearity of the absorption with sample pressure. The measured absorption cross

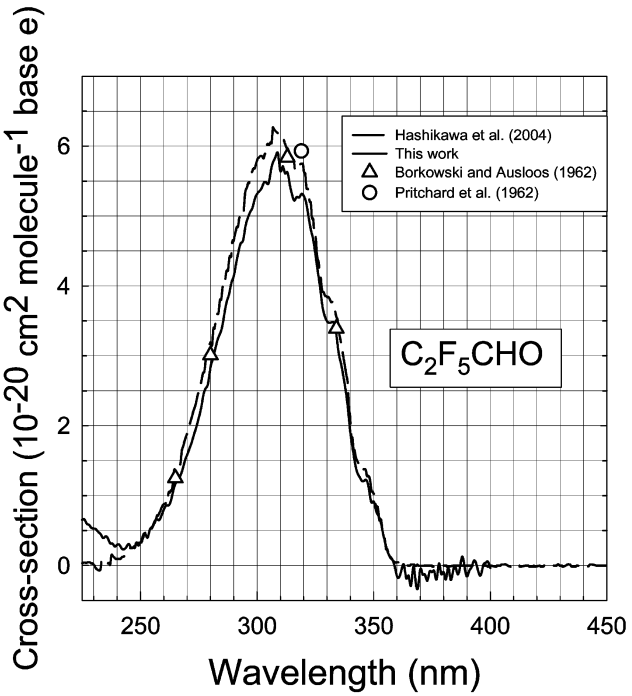

Figure 2. UV absorption cross sections for C_2F_5CHO from Hashikawa et al.[33] (dashed line), Borkowski and Ausloos (triangles),[29] Pritchard et al. (circles),[34] and the present work (solid line).

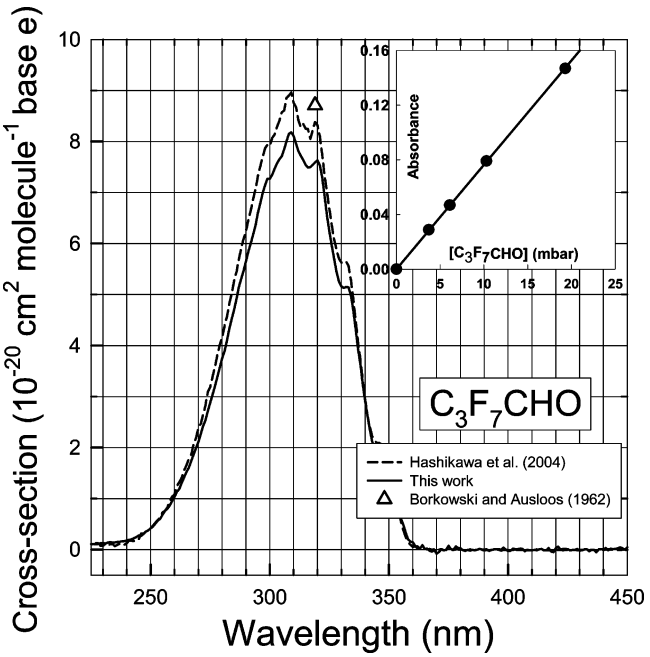

Figure 3. UV absorption cross sections for C_3F_7CHO from Hashikawa et al.(dashed line),[33] Borkowski and Ausloos (triangles),[29] and the present work (solid line). The insert shows the calibration curve (300 nm).

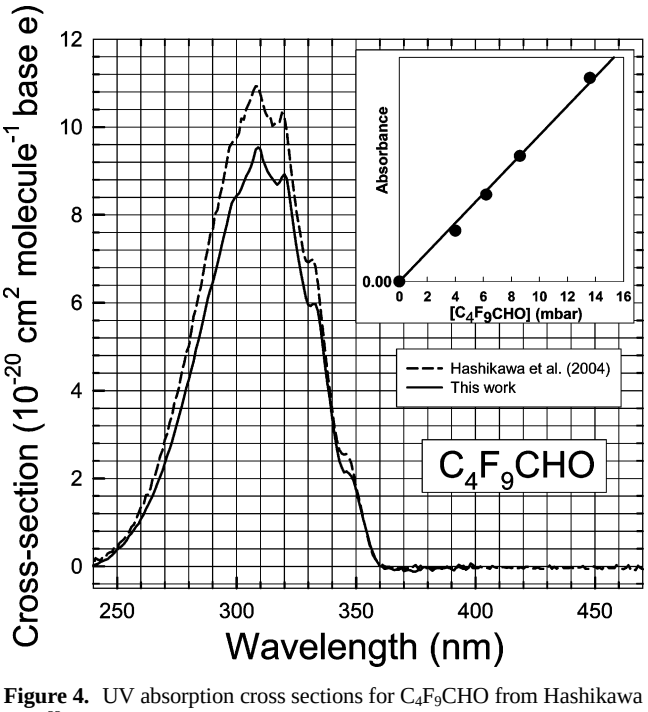

Figure 4. UV absorption cross sections for C_4F_9CHO from Hashikawa et al.[33] (dashed line) and the present work (solid line). The insert shows the calibration curve.

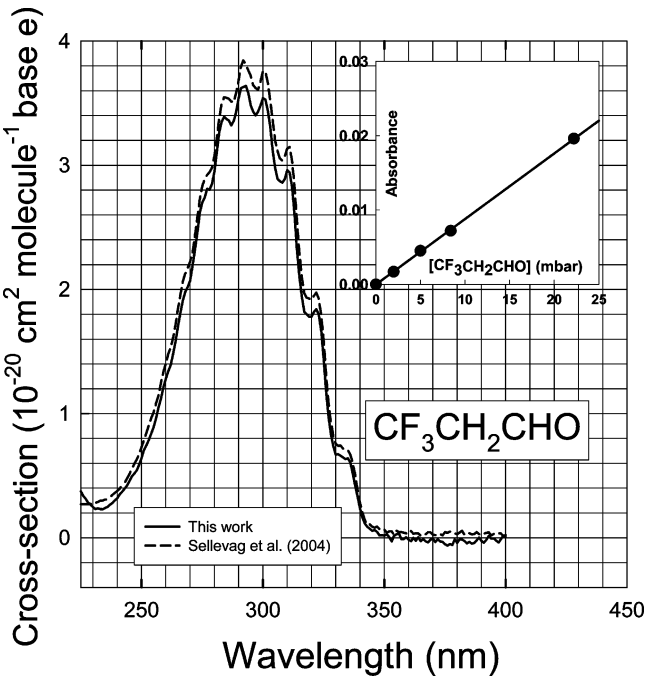

Figure 5. UV absorption cross sections for CF_3CH_2CHO from Sellevåg et al.[21] (dashed line) and the present work (solid line). The insert shows the calibration curve.

sections are listed in 5 nm intervals in Table 1 and in 1 nm intervals in the Supporting Information. Accounting for the experimental reproducibility (6%) and systematic uncertainties associated with pressure measurements (2%), UV path length (1%), and sample purity (1%), we estimate that the absorption cross sections have an accuracy of ±10%. As discussed in the previous section, as a result of its low vapor pressure it was only possible to use one relatively low partial pressure sample (1.5 mbar) of $C_6F_{13}CH_2CHO$. This sample had a relatively small absorbance, and hence, we assign a larger uncertainty (±15%) for this spectrum.

The absorption cross sections reported previously for the fluorinated aldehydes studied in the present work are compared with the results from the present work in Figures 1−6. There is good agreement (within 10%) between the results of previous studies of the UV absorption cross sections of CF_3CHO,[21,29−33] C_2F_5CHO,[29,33,34] and C_3F_7CHO[29,33] and the results from the present work. As shown in Figure 4, the spectrum of C_4F_9CHO measured in the present work lies below (average of 13% difference in absorption cross sections at 280−340 nm) but is consistent, within the combined experimental uncertainties, with that reported by Hashikawa et al.[33] The spectrum of

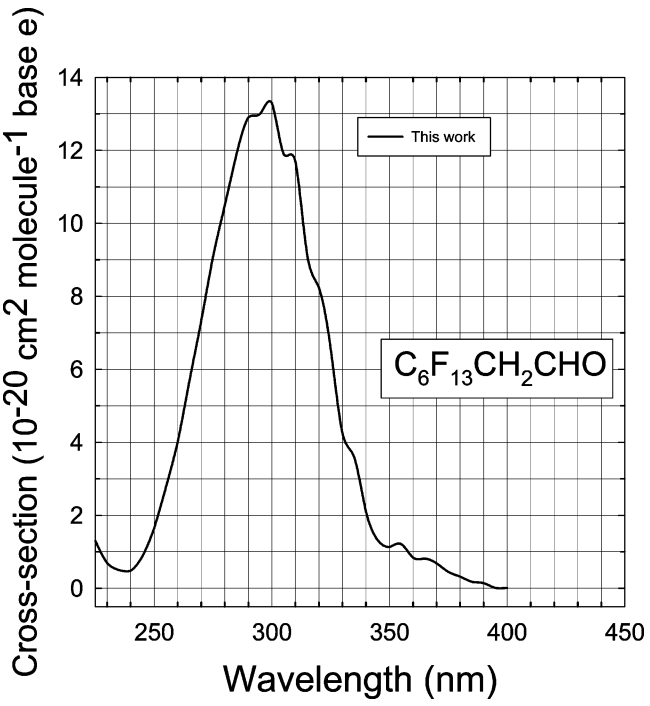

Figure 6. UV absorption cross sections for $C_6F_{13}CH_2CHO$ measured in the present work.

CF_3CH_2CHO is in good agreement (average of 6% difference in absorption cross sections at 270−320 nm) with the previous work of Sellevåg et al.[21] Our spectrum of $C_6F_{13}CH_2CHO$ is the first reported for this compound. Finally, we note that a spectrum for CF_3CHO reported by Lucazeau and Sandorfy[30] is similar in shape to those in Figure 1 but is approximately 30% less intense and is not considered further here.

As discussed previously,[33] $C_xF_{2x+1}CHO$ have a broad UV absorption centered at 300−310 nm; there is a slight red shift in the absorption maximum in moving from CF_3CHO to C_2F_5CHO but little or no additional shift for the larger members of the series. There is a substantial increase in the strength of absorption with increasing size of $C_xF_{2x+1}CHO$. Comparison of the spectra of CF_3CH_2CHO and $C_6F_{13}CH_2CHO$ in Figures 5 and 6 shows that there is little or no red shift but there is a substantial increase in absorption strength with increasing size of $C_xF_{2x+1}CH_2CHO$. The spectrum of $C_6F_{13}CH_2CHO$ is approximately 3.5 times more intense than that of CF_3CH_2CHO.

3.2. UV Absorption Spectra at 249, 265, 281 K. To investigate the effect of temperature, UV spectra for CF_3CHO, C_2F_5CHO, C_3F_7CHO, C_4F_9CHO, and CF_3CH_2CHO were recorded at 249, 265, and 281 K. Representative data are shown for CF_3CH_2CHO in Figure 7. Low-temperature spectra for CF_3CHO, C_2F_5CHO, C_3F_7CHO, and C_4F_9CHO are given in Figures S1−4 in the Supporting Information. In all cases, within the experimental uncertainties, there was no discernible systematic effect of variation of temperature over the range 249−297 K in the UV absorption spectra. Given the absence of a discernible temperature effect, the spectra obtained at 297 K discussed in the previous section can be used in atmospheric models to calculate photolysis rates.

3.3. Photolysis Quantum Yields at 308 nm. The quantum yields for photolysis of CF_3CHO, CF_3CH_2CHO, C_4F_9CHO, and $CH_3C(O)CH_3$ were measured relative to that for CH_3CHO in 700 Torr of N_2 diluent. Reaction mixtures consisted of 1−5 Torr of the carbonyl compound and 10−50 Torr of NO in 700 Torr of N_2 diluent. NO was added to scavenge the radical products formed in the photodissociation of the carbonyl compound, which might otherwise contribute to unwanted secondary loss of the carbonyl compound. The reaction mixtures were exposed to up to 12 000 pulses (approximately 70 mJ pulse^{-1}) of 308 nm photons from a XeCl laser operated at a repetition rate of 10 Hz. Following exposure of the sample to a predetermined number of laser pulses, the cell was transferred to the sample compartment of an FTIR spectrometer for analysis. The transfer procedure took approximately 10 min. Control experiments were conducted to check for effects of (i) the orientation of the sample cell in the laser beam and (ii) the laser repetition rate. Rotating the sample cell by 180° to switch the direction in which the laser beam traverses the cell and reduction in the laser repetition rate by a factor of 5 had no discernible effect on the results.

As discussed in section 2.1, NO was added to the gas mixtures to scavenge the photolysis products and avoid loss of aldehydes by unwanted chemistry. For example, the photolysis of CF_3CHO is expected to give CF_3 radicals which, in the absence of NO, may abstract hydrogen from CF_3CHO leading to formation of CF_3H and additional loss of CF_3CHO. Formation of CF_3H in this process could be confused with the direct formation of this product as a primary photolysis product. CF_3H has a long tropospheric lifetime, a large global warming potential, and if formed as a product of the atmospheric photolysis of CF_3CHO would be of significance. Figure 8 shows a plot of the formation of CF_3NO versus loss of CF_3CHO observed following the pulsed radiolysis of $CF_3CHO/NO/N_2$ mixtures. The line through the data gives a CF_3NO yield of 98 ± 7%. Features attributable to CF_3H were searched for but not found, and an upper limit of <2% was established for the yield of this species. The observation of CF_3NO product in a yield which is indistinguishable from 100% is consistent with expectations based upon analogy with CH_3CHO that the 308 nm photolysis of CF_3CHO proceeds essentially exclusively via C−C bond scission

$$CF_3CHO + h\nu \rightarrow CF_3 + HCO \quad (1a)$$

$$CF_3CHO + h\nu \rightarrow CF_3H + CO \quad (1b)$$

$$CF_3 + NO + M \rightarrow CF_3NO + M$$

In similar experiments involving C_2F_5CHO, C_3F_7CHO, and C_4F_9CHO, there was no evidence (<5% yield) for the formation of C_2F_5H, C_3F_7H, and C_4F_9H. We conclude that formation of HFCs from the tropospheric photolysis of fluoroaldehydes is of no significance.

As shown in Figure 9, semilog plots of the decay of the carbonyl compound versus the number of laser pulses (i.e., irradiation time) are linear, indicating that the photolysis is a first-order process. A power meter was used to record the power of each laser pulse after it has traversed the reaction cell. Small corrections have been applied to the data in Figure 9 to account for minor (<10%) fluctuations in the average pulse power between different experiments. The lines through the data in Figure 9 are linear least-squares fits. A potential complication in the present work is the fact that the excimer laser pulse irradiates only approximately one-fifth of the reaction cell. We assume that mixing (diffusion and convection) within the cell provides uniform irradiation of the gas mixtures during an experiment. The substantial consumptions of the samples (up to 58% consumption for CH_3CHO) and linearity of the plots in Figure 9 suggest that this assumption is valid. The slopes of these lines contain information concerning the relative photolysis rates of the compounds when exposed to 308 nm radiation.

TABLE 1: Absorption Cross Sections (10^{-20} cm^2 molecule^{-1}) Measured at 297 K

wavelength	CF_3CHO	C_2F_5CHO	C_3F_7CHO	C_4F_9CHO	CF_3CH_2CHO	$C_6F_{13}CH_2CHO$
230	0.10	0.53	0.12	0	0.25	0.69
235	0.11	0.39	0.15	0	0.24	0.50
240	0.13	0.28	0.18	0.021	0.32	0.48
245	0.19	0.27	0.26	0.15	0.46	0.88
250	0.32	0.36	0.42	0.37	0.65	1.65
254	0.46	0.51	0.60	0.59	0.84	2.31
255	0.50	0.55	0.68	0.68	0.91	2.77
260	0.72	0.78	1.03	1.09	1.27	4.02
265	0.99	1.13	1.51	1.64	1.70	5.69
270	1.30	1.58	2.13	2.35	2.12	7.33
275	1.64	2.13	2.88	3.24	2.67	9.08
280	1.98	2.80	3.74	4.26	2.99	10.5
285	2.31	3.46	4.72	5.38	3.36	11.9
290	2.60	4.17	5.66	6.49	3.52	12.9
295	2.80	4.83	6.59	7.59	3.51	13.0
300	2.89	5.29	7.30	8.43	3.48	13.3
305	2.84	5.57	7.76	9.00	3.03	11.9
308	2.72	5.86	8.15	9.49	2.86	11.6
310	2.68	5.74	8.04	9.38	2.89	11.7
315	2.40	5.38	7.58	8.83	2.16	9.14
320	2.04	5.21	7.52	8.77	1.80	8.24
325	1.67	4.43	6.28	7.33	1.41	6.57
330	1.27	3.55	5.23	6.07	0.72	4.25
335	0.93	3.08	4.62	5.38	0.61	3.59
340	0.56	1.96	2.95	3.40	0.25	2.10
345	0.34	1.25	1.96	2.21	0.065	1.32
350	0.19	0.88	1.52	1.71	0.018	1.13
355	0.03	0.35	0.64	0.68	0.007	1.21
360	0.01		0.13	0.041		0.84
365			0.024			0.81
370						0.68

As discussed in section 2.1, CH_3CHO was chosen as the chemical actinometer in the present system. As a check of the experimental techniques prior to investigation of the photolysis of the fluorinated aldehydes, the photolysis of $CH_3C(O)CH_3$ was studied. As seen from Figure 9, photolysis of $CH_3C(O)CH_3$ proceeds more slowly than that of CH_3CHO. The ratio of the slopes of the $CH_3C(O)CH_3$ and CH_3CHO data in Figure 9 is $(1.65 \pm 0.12) \times 10^{-5}/(1.08 \pm 0.09) \times 10^{-4} = 0.153 \pm 0.017$. This can be compared to the ratio expected on the basis of the recommended data for the absorption cross sections and photolysis quantum yields for $CH_3C(O)CH_3$ and CH_3CHO at 308 nm; $(\sigma_{CH_3C(O)CH_3} \times \phi_{CH_3C(O)CH_3})/(\sigma_{CH_3CHO} \times \phi_{CH_3CHO}) = (1.66 \times 10^{-20} \times 0.116)/ (3.33 \times 10^{-20} \times 0.322) = 0.180 \pm 0.028$ (uncertainties were estimated assuming 5% uncertainty in $\sigma_{CH_3C(O)CH_3}$ and σ_{CH_3CHO} and 10% uncertainty in $\phi_{CH_3C(O)CH_3}$ and ϕ_{CH_3CHO}). The consistency of the observed relative photolysis rates of $CH_3C(O)CH_3$ and CH_3CHO with expectations based upon the IUPAC recommended absorption cross sections and photolysis quantum yields provides confidence in the present experimental methodology.

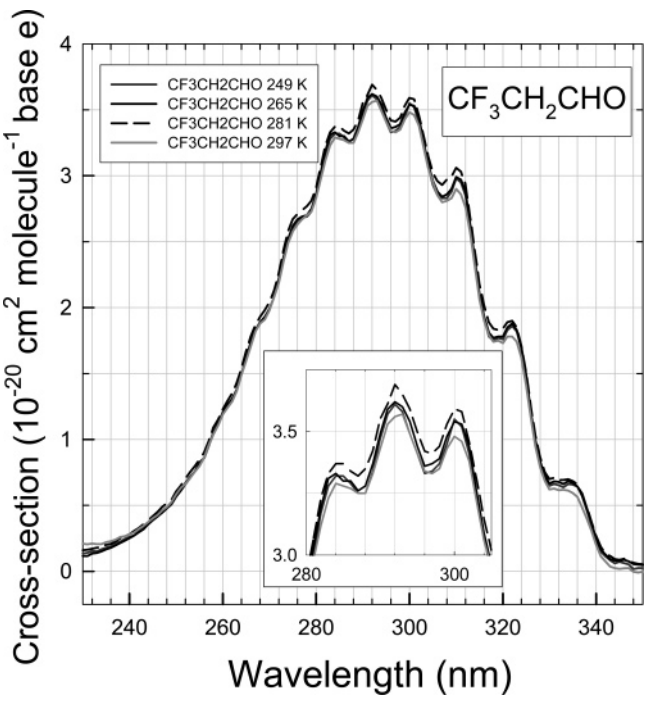

Figure 7. UV spectra of CF_3CH_2CHO at 249, 265, 283, and 297 K. The insert shows the spectrum near the peak absorption; the axes units are the same as the larger plot.

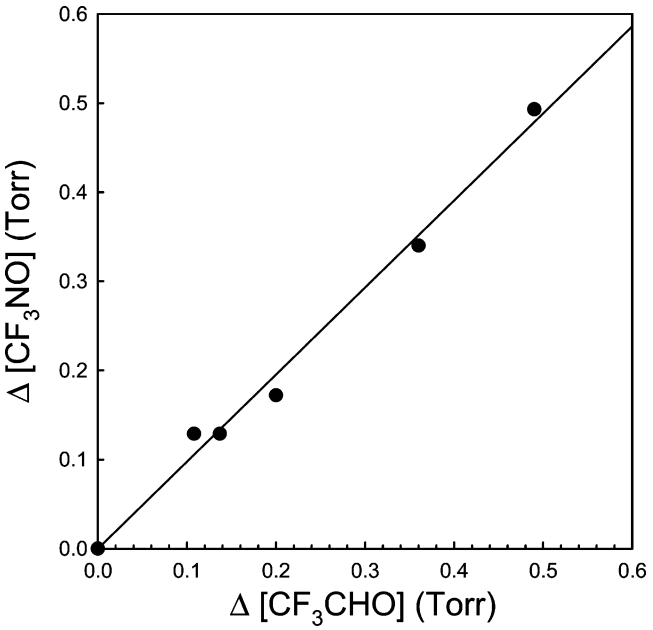

Figure 8. Formation of CF_3NO vs loss of CF_3CHO following 308 nm irradiation of $CF_3CHO/NO/N_2$ mixtures.

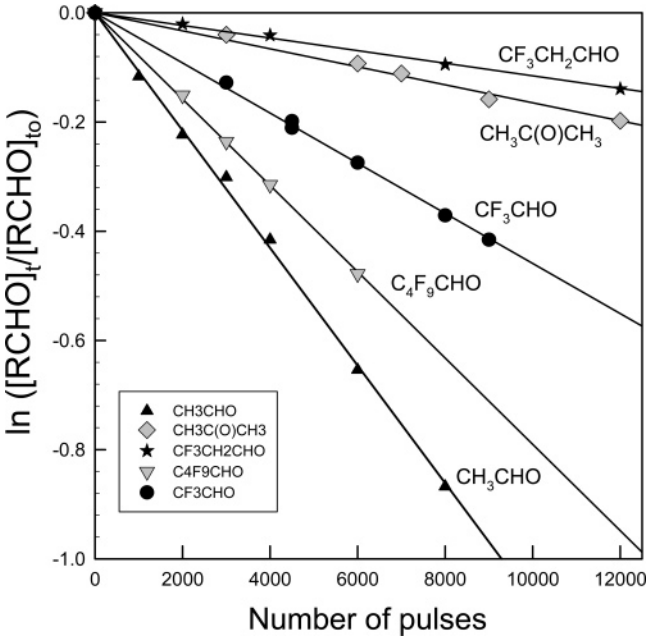

Figure 9. Decay of CH_3CHO, CF_3CHO, C_4F_9CHO, CF_3CH_2CHO, and $CH_3C(O)CH_3$ vs number of laser pulses following exposure to 308 nm pulses from an excimer laser (see text for details).

In addition to considering the relative rates of photolysis, we can also compare the absolute rates with expectations based upon the IUPAC recommended data. Thus, taking $\sigma_{CH_3C(O)CH_3} = 1.66 \times 10^{-20}$ molecule cm^{-2} and $\phi_{CH_3C(O)CH_3} = 0.116$, we can estimate the loss of CH_3CHO expected upon exposure to UV irradiation. The excimer laser beam profile was approximately 2.5 × 1.1 cm. Consider the experiment shown in Figure 9 in which a mixture of 5.0 Torr of $CH_3C(O)CH_3$ and 51.6 Torr of NO in 700 Torr total pressure of N_2 diluent was exposed to 6000 laser pulses. The average energy of the laser pulses in the cell was approximately 70 mJ $pulse^{-1}$ (see section 2.1). The average number of 308 nm photons transmitted through the cell was 1.09×10^{17} per pulse (3.95×10^{16} photons cm^{-2} $pulse^{-1}$). Considering a 1 cm^3 volume within the laser beam, $[CH_3C(O)CH_3] = 1.62 \times 10^{17}$, OD = σ c l = 2.69×10^{-3}, and 1.06×10^{14} photons are absorbed in the 1 cm^3 volume during each laser pulse. Using $\phi_{CH_3C(O)CH_3} = 0.116$, it follows that 1.23×10^{13} $CH_3C(O)CH_3$ molecules are photolyzed each pulse. After 6000 pulses, the consumption of $CH_3C(O)CH_3$ will be 7.38×10^{16} molecules. In comparison to the initial $[CH_3CHO]$ and accounting for the fact that the laser beam illuminates approximately 20% of the reaction cell volume, it is estimated that approximately 8% of the CH_3CHO is photolyzed. This estimate is consistent with the 9% observed loss of $CH_3C(O)CH_3$ in this experiment. The consistency between the estimated and measured loss of $CH_3C(O)CH_3$ is gratifying and provides support for the experimental methodology.

The lines through the CF_3CHO, C_4F_9CHO, and CF_3CH_2CHO data in Figure 9 are linear least-squares fits which have slopes of $(4.7 \pm 0.5) \times 10^{-5}$, $(7.9 \pm 0.9) \times 10^{-5}$, and $(1.2 \pm 0.1) \times 10^{-5}$. Using the absorption cross sections measured in the present work, we derive quantum yields for photolysis of CF_3CHO, C_4F_9CHO, and CF_3CH_2CHO in 700 Torr of N_2 at 296 K of 0.17 ± 0.03, 0.08 ± 0.02, and 0.04 ± 0.01, respectively. These values are listed in Table 2.

3.4. Photolysis Quantum Yields at 254 nm. The quantum yields for photolysis of CF_3CHO, C_2F_5CHO, C_3F_7CHO, C_4F_9CHO, CF_3CH_2CHO, and $C_6F_{13}CH_2CHO$ were measured using perfluoroacetic anhydride as a chemical actinometer.[27]

TABLE 2: Quantum Yields Measured in the Present Work

	Quantum Yields			
	$\lambda = 254$ nm			$\lambda = 308$ nm
sample	ϕ_{Total}	ϕ_{2a}	ϕ_{2b}	ϕ_{Total}
CF_3CHO	0.79 ± 0.09	0.41 ± 0.07	0.38 ± 0.07	0.17 ± 0.03
C_2F_5CHO	0.81 ± 0.09	0.38 ± 0.08	0.43 ± 0.08	
C_3F_7CHO	0.63 ± 0.09	0.31 ± 0.07	0.32 ± 0.07	
C_4F_9CHO	0.60 ± 0.09	0.31 ± 0.08	0.29 ± 0.07	0.08 ± 0.02
CF_3CH_2CHO	0.74 ± 0.08	0.38 ± 0.09	0.36 ± 0.07	0.04 ± 0.01
$C_6F_{13}CH_2CHO$	0.55 ± 0.09			

Reaction mixtures consisted of 0.5−5.5 mbar of the carbonyl compound and 20−70 mbar of NO (added as a radical scavenger; see section 2.1). Irradiation of the gas mixtures using the output from a low-pressure Hg lamp for 5−100 minutes led to a loss of the carbonyl compounds. Control experiments were performed to check for loss when the sample compounds were allowed to sit in the cell in the dark for up to 2 h; there was no discernible (<1%) loss. Figure 10 shows a semilog plot of sample concentration versus time; the linearity of the data shows that the decay of the samples follows first-order kinetics. The lines through the data are linear least-squares fits which give pseudo first-order loss rates of $(7.1 \pm 0.3) \times 10^{-4}$, $(8.1 \pm 0.6) \times 10^{-4}$, $(7.4 \pm 0.4) \times 10^{-4}$, $(7.0 \pm 0.6) \times 10^{-4}$, $(1.2 \pm 0.1) \times 10^{-3}$, $(2.5 \pm 0.4) \times 10^{-3}$, and $(1.30 \pm 0.01) \times 10^{-2}$ min^{-1} for CF_3CHO, C_2F_5CHO, C_3F_7CHO, C_4F_9CHO, CF_3CH_2CHO, $C_6F_{13}CH_2CHO$, and $(CF_3C(O))_2O$, respectively. The errors are 2 standard deviations. Quantum yields listed in Table 2 were calculated from the ratio of the slopes $k_{C_xF_{2x+1}CHO}/k_{(CF_3C(O))_2O} = \sigma_{C_xF_{2x+1}CHO} \times \phi_{C_xF_{2x+1}CHO}/(\sigma_{(CF_3C(O))_2O} \times \phi_{(CF_3C(O))_2O})$ (uncertainties were estimated assuming 10%, 5%, and 7% uncertainty in $\sigma_{C_xF_{2x+1}CHO}$, $\sigma_{(CF_3C(O))_2O}$, and $\phi_{(CF_3C(O))_2O}$, respectively). The aldehyde absorption cross sections measured in this work (Table 1) and literature data[27] for the absorption cross section and photolysis quantum yield for perfluoroacetic anhydride were used (see section 2.1).

Irradiation of RCHO/NO mixtures at 254 nm led to the formation of two observable products; the corresponding nitrosyl (RNO) and the hydrofluorocarbon (RH). The yields of the

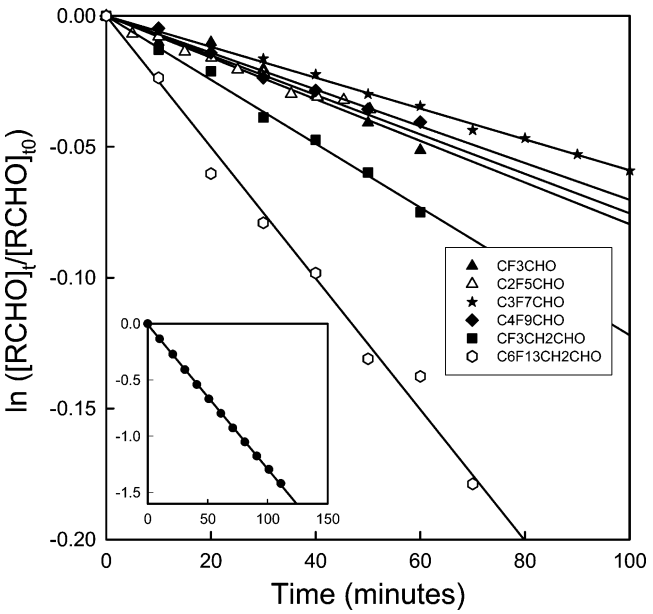

Figure 10. Decay of CH_3CHO, CF_3CHO, C_4F_9CHO, CF_3CH_2CHO, and $C_6F_{13}CH_2CHO$ vs time of exposure to 254 nm radiation. The inset shows data for perfluoroacetic anhydride (used as chemical actinometer).

nitrosyl and hydrofluorocarbon products contain information on the quantum yields for processes 2a and 2b.

$$C_xF_{2x+1}CHO + h\nu \rightarrow C_xF_{2x+1} + HCO \quad (2a)$$

$$C_xF_{2x+1}CHO + h\nu \rightarrow C_xF_{2x+1}H + CO \quad (2b)$$

Reference spectra for CF_3NO and C_4F_9NO were available and were used to quantify the formation of these species. The formation of other nitrosyl compounds ($C_xF_{2x+1}NO$ and $C_xF_{2x+1}CH_2NO$) was quantified by assuming that the oscillator strength of the −NO stretching at around 1600 cm^{-1} is independent of the alkyl group in the molecule. The IR spectrum of C_4F_9NO is shown in Figure S5 in the Supporting Information. Reference spectra for CF_3H, CF_3CH_3, C_2F_5H, and C_3F_7H were used to quantify the formation of these species. The low volatility of $C_6F_{13}CH_2CHO$ precluded the use of reactant pressures sufficient to make reliable product determinations. The quantum yields for processes 2a and 2b derived in this work are given in Table 2. The present work shows that, at 254 nm, the molecular channel giving HFCs becomes an important photolysis pathway.

3.5. Estimation of Atmospheric Photolysis Rates. The *Tropospheric Ultraviolet−Visible* (TUV 4.2) package[35] was used to estimate the rates of photolysis of CF_3CHO, C_2F_5CHO, C_3F_7CHO, C_4F_9CHO, CF_3CH_2CHO, and $C_6F_{13}CH_2CHO$ within the troposphere. The program was run assuming a cloudless sky, a surface albedo of 0.1, and 300 DU ozone column. The UV spectra and quantum yields reported herein were used in the calculations. Ideally, in such calculations wavelength-dependent quantum yields should be used. However, such data are not available, and hence, we assumed wavelength-independent values. The sensitivity of our conclusions to this assumption is discussed at the end of this section. Quantum yields for the photolysis of C_2F_5CHO, C_3F_7CHO, and $C_6F_{13}CH_2CHO$ are not available. It seems reasonable to assume that the quantum yields for C_2F_5CHO and C_3F_7CHO will lie between those for CF_3CHO and C_4F_9CHO. Quantum yield (ϕ) values for C_2F_5CHO and C_3F_7CHO were estimated by interpolation from the data for CF_3CHO and C_4F_9CHO. The ϕ value for $C_6F_{13}CH_2CHO$ was estimated assuming that ϕ is inversely proportional to molecular size and follows the same trend as observed for CF_3CHO and C_4F_9CHO. The quantum yield for photolysis of C_4F_9CHO is a factor of approximately 2 lower than that for CF_3CHO. The change in molecular size from CF_3CH_2CHO to $C_6F_{13}CH_2CHO$ is approximately a factor of 2 larger than from CF_3CHO to C_4F_9CHO. Hence, we proceed on the assumption that $\phi_{C_6F_{13}CH_2CHO} = 0.25 \times \phi_{CF_3CH_2CHO} = 0.01$. It should be emphasized that these estimation procedures are crude, and further experimental measurements are critical in this area.

The quantum yields used in the modeling were 0.17 (CF_3CHO), 0.14 (C_2F_5CHO), 0.11 (C_3F_7CHO), 0.08 (C_4F_9CHO), 0.04 (CF_3CH_2CHO), and 0.01 ($C_6F_{13}CH_2CHO$). Photolysis lifetimes (24 h average) were calculated with the TUV model at 40° latitude for the summer and winter solstices and the fall and spring equinoxes. The results were averaged to provide an estimate of the annual average. Figure 11 shows a plot of the estimated annual average lifetimes of CF_3CHO, C_2F_5CHO, C_3F_7CHO, C_4F_9CHO, CF_3CH_2CHO, and $C_6F_{13}CH_2CHO$ with respect to photolysis. As seen from Figure 11, the lifetime of the fluorinated aldehydes with respect to photolysis is short (<2 days for C_2F_5CHO, C_3F_7CHO, and C_4F_9CHO), while for the telomer aldehydes, it is around an order of magnitude longer. For comparison, it has been estimated that the atmospheric lifetime of $C_xF_{2x+1}CHO$ and $C_xF_{2x+1}CH_2CHO$ with respect to reaction with OH radicals are approximately 26 and 4 days, respectively.[21] The lifetime of $C_xF_{2x+1}CHO$ with respect to reaction with water to form the hydrate appears to be limited by the time scale for air within the atmosphere to come in contact with a liquid water surface[36] (order of 5−10 days[37,38]). We conclude that photolysis is the dominant atmospheric fate of $C_xF_{2x+1}CHO$ ($x = 1-4$) and is an important fate for $C_xF_{2x+1}CH_2CHO$ ($x = 1$ and 6).

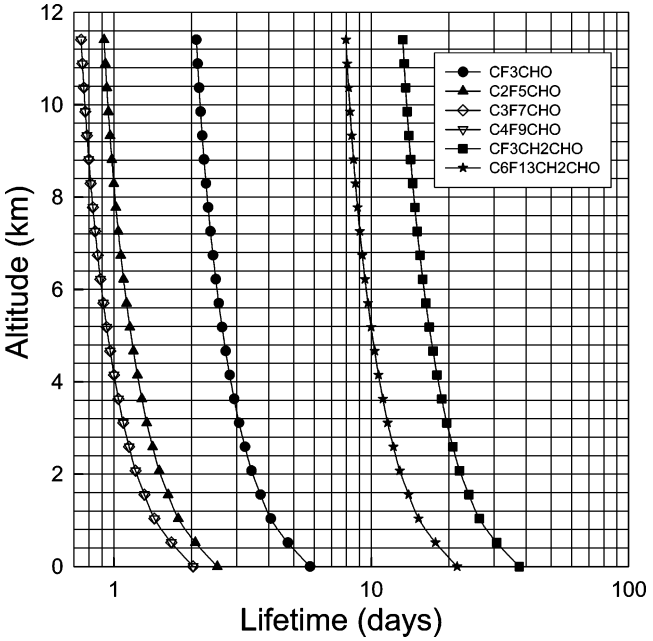

Figure 11. Atmospheric lifetimes of CF_3CHO, C_2F_5CHO, C_3F_7CHO, C_4F_9CHO, CF_3CH_2CHO, and $C_6F_{13}CH_2CHO$ with respect to photolysis in the lower atmosphere.

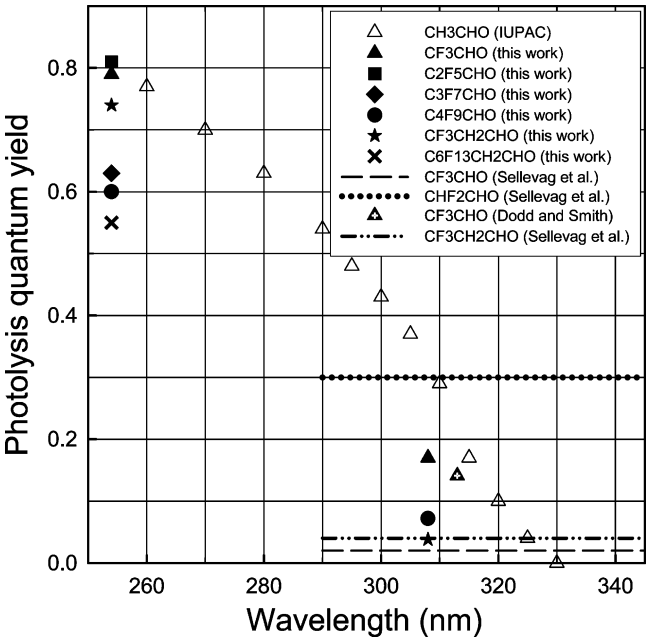

Figure 12. Quantum yields measured in the present and previous studies of fluoroaldehydes.

Finally, we need to discuss our assumption of wavelength-independent quantum yields and the fact that in reality the quantum yields will be dependent on wavelength. As illustrated by the CH_3CHO data in Figure 12, it is expected that the photolysis quantum yields for the fluorinated aldehydes will decrease with increasing wavelength. In the approach used in

the present work, photolysis following absorption at wavelengths of >308 nm will be overestimated, while photolysis following absorption at wavelengths of <308 nm will be underestimated. The use of a quantum yield measured at 308 nm near the peak of the UV absorption reduces, but does not eliminate, the uncertainties in the photolysis lifetimes associated with the assumption of wavelength-independent quantum yields. To provide insight into the likely impact of the effect of variation of quantum yield with wavelength, additional calculations were performed for CF_3CHO. Using the behavior of CH_3CHO as a guide, we arbitrarily assumed that the quantum yield of CF_3CHO decreased linearly with wavelength from 254 (ϕ = 0.79) to 308 nm (ϕ = 0.17) and from 308 to reach ϕ = 0 at 340 nm. Including this wavelength dependence led to a decrease in the calculated rate of photolysis by a factor of approximately 2.8. While the wavelength dependence of ϕ is an important parameter which needs to be measured, its inclusion in future model calculations is not likely to change the main conclusion in the present work that photolysis is an important atmospheric loss for the fluoroaldehydes.

4. Discussion

4.1. UV Spectra. The UV spectra for CF_3CHO, C_2F_5CHO, C_3F_7CHO, C_4F_9CHO, and CF_3CH_2CHO measured in the present work at 297 K are slightly less intense but are consistent, within the combined experimental uncertainties, with the previous measurements. The measurements at subambient temperature are the first to be reported and show that there is no significant (<5%) temperature effect over the atmospherically relevant range. The present work confirms the increased intensity of the UV spectra of $C_xF_{2x+1}CHO$ with increasing molecular size. A steady progression is observed with the spectra of CF_3CHO, C_2F_5CHO, C_3F_7CHO, and C_4F_9CHO having similar shapes but with the strength of the absorption increasing with molecular size. The present work shows that a similar effect is evident for $C_xF_{2x+1}CH_2CHO$ with the spectrum of $C_6F_{13}CH_2CHO$ being approximately 3.5 times more intense than that of CF_3CH_2CHO. Absorption by $C_xF_{2x+1}CH_2CHO$ occurs at longer wavelengths than for $C_xF_{2x+1}CHO$, and this is the main factor accounting for the shorter photolytic lifetimes of $C_xF_{2x+1}CH_2CHO$ in the troposphere.

4.2. Quantum Yields. The quantum yields measured here are compared to literature data for acetaldehyde and fluorinated aldehydes in Figure 12. The quantum yield data for CH_3CHO plotted in Figure 12 are those recommended by the IUPAC data panel in 1 atm of air diluent.[28] At a wavelength of 254 nm (measured in the presence of 25−70 mbar of NO), our measured photolysis quantum yields for CF_3CHO and C_2F_5CHO are indistinguishable from that of CH_3CHO in 1 atm of air. The quantum yields for C_3F_7CHO and C_4F_9CHO are smaller than those for CF_3CHO and C_2F_5CHO, presumably reflecting the increased number of degrees of freedom of the larger aldehydes over which to distribute the excitation energy, the longer lifetime of the excited species, and hence the increased opportunity for collisional quenching. As seen from Table 2, we find that at 254 nm the quantum yields ϕ_{2a} and ϕ_{2b} for the two different photolysis channels are indistinguishable within the experimental uncertainties. This finding is consistent with the report by Morris and Thynne[39] that processes 2a and 2b are of comparable importance in the unfiltered medium-pressure Hg arc lamp photolysis of C_2F_5CHO.

As seen in Figure 12, there is a trend of decreasing photolysis quantum yield with increasing molecular size evident in the data measured in the present study using 254 and 308 nm radiation. The decreased efficiency of photolysis presumably reflects the greater number of degrees of freedom in the larger molecules over which to distribute the excitation energy, leading to a longer lifetime of the excited state and a greater chance of collisional deactivation.

The photolysis of CF_3CHO has been studied previously by Dodd and Smith,[40] Pearce and Whytock,[41] Morris and Thynne,[40] Richter et al.,[42] and Sellevåg et al.[21] Dodd and Smith used 313 nm photolysis light and estimated quantum yields of 0.021 for the $CF_3H + CO$ channel and 0.12 for the $CF_3 + HCO$ channel. The quantum yield for CF_3H formation of 0.021 is slightly larger than the upper limit of <0.02 derived in the present work. The combined quantum yield reported by Dodd and Smith is plotted in Figure 12 and is consistent with the results from the present work. Pearce and Whytock investigated the $CF_3H + CO$ channel (313 nm photolysis light) and concluded that it had a quantum yield of zero. Pearce and Whytock ascribed the discrepancy between their result and that of Dodd and Smith to either errors in the light intensity calibration or the presence of photolysis light of wavelengths <313 nm in the study by Dodd and Smith. Richter et al. irradiated CF_3CHO/air mixtures using either 253.7 or 366 nm UV radiation. The products observed following 253.7 nm irradiation were CF_3H (14%), CF_2O (80%), CO (60%), and CO_2 (45%). The observation of CF_3H products shows that the $CF_3H + CO$ channel is important in the 253.7 nm photolysis. Considering the likely contribution of reaction with CF_3O radicals to the CF_3CHO loss, the observed 14% CF_3H yield provides a lower limit for $\phi_{2b}/(\phi_{2a} + \phi_{2b}) > 0.14$. Our determination of $\phi_{2b}/(\phi_{2a} + \phi_{2b}) = 0.48 \pm 0.09$ is consistent with the previous observations of Richter et al. Experiments by Richter et al. using 366 nm UV radiation did not produce any substantial loss of CF_3CHO. This is not surprising considering that there is little or no absorption by CF_3CHO at 366 nm.

Sellevåg et al.[21] introduced CF_3CHO samples into the EUPHORE outdoor smog chamber in one atmosphere of air and exposed the mixtures to sunlight. SF_6 inert tracer was used to quantify leaks from the chamber. The decay rates of CF_3CHO and SF_6 were indistinguishable, and Sellevåg et al.[21] derived an upper limit of $\phi < 0.02$ for the effective photolysis quantum yield at 290−400 nm. In similar experiments, Sellevåg et al.[21] derived an upper limit of $\phi < 0.04$ for the effective photolysis quantum yield at 290−400 nm for CF_3CH_2CHO. In a more recent study, Sellevåg et al.[20] studied CHF_2CHO in the EUPHORE chamber and reported an effective photolysis quantum yield at 290−500 nm, $\phi = 0.30 \pm 0.05$.

As seen from inspection of Figure 12, the quantum yield for CHF_2CHO photolysis reported by Sellevåg et al.[20] is similar to the literature data for photolysis of CH_3CHO but very different from the upper limit for CF_3CHO reported by Sellevåg et al.[20] This raises the question, "Why does addition of two fluorine atoms have little effect, but addition of a third fluorine atom has a large effect?" Sellevåg et al.[20] addressed this question in a computational study. Their calculations showed that the excited state of CF_3CHO has a low dissociative barrier, and hence, the photolysis quantum yield should be significant. Rather than questioning their experimental results, Sellevåg et al.[20] chose to "look for a different interpretation" of the computational data. Sellevåg et al.[20] speculated that possible low-lying intersections between the electronic states involved in the photodissociation processes explain the experimental observations. As seen from Figure 12, the results from the present study at 308 nm and that of Dodd and Smith at 313 nm are inconsistent with the upper limit reported by Sellevåg et al.[21] The simplest explanation of the discrepancy between the experimental results of Sellevåg

et al.[21] and (i) the data from Dodd and Smith, (ii) the results from the present work, and (iii) the computational findings by Sellevåg et al.[20] is that the experimental measurements of the CF_3CHO quantum yield by Sellevåg et al.[21] are, for reasons which are unclear, in error.

4.3. Atmospheric Lifetimes and Environmental Implications. The results from the present work have important implications for our understanding of the atmospheric oxidation mechanism of fluorotelomer alcohols. Our results indicate that photolysis is an important atmospheric loss mechanism for perfluoroaldehydes ($C_xF_{2x+1}CHO$) and fluorotelomer aldehydes ($C_xF_{2x+1}CH_2CHO$). As seen from Figure 11 and discussed in section 3.4, the atmospheric lifetimes of $C_xF_{2x+1}CHO$ ($x = 1-4$) with respect to photolysis are short, and photolysis probably dominates their atmospheric fate. The atmospheric lifetimes of $C_xF_{2x+1}CH_2CHO$ ($x = 1, 6$) with respect to photolysis are longer than those for $C_xF_{2x+1}CHO$ ($x = 1-4$). While photolysis is *not* the dominant atmospheric loss mechanism for $C_xF_{2x+1}CH_2CHO$ ($x = 1, 6$), it does make a significant contribution.

Current interest in the atmospheric chemistry of perfluoroaldehydes, $C_xF_{2x+1}CHO$, centers on their potential role as intermediates in the formation of perfluorocarboxylic acids ($C_xF_{2x+1}COOH$) during the atmospheric oxidation of fluorotelomer alcohols. Two gas-phase mechanisms by which $C_xF_{2x+1}CHO$ can be transformed into $C_xF_{2x+1}COOH$ have been proposed:[13] first, conversion into $C_xF_{2x+1}C(O)O_2$ followed by reaction with HO_2

$$C_xF_{2x+1}CHO + OH \rightarrow C_xF_{2x+1}CO + H_2O$$

$$C_xF_{2x+1}CO + O_2 + M \rightarrow C_xF_{2x+1}C(O)O_2 + M$$

$$C_xF_{2x+1}C(O)O_2 + HO_2 \rightarrow C_xF_{2x+1}COOH + M$$

and second, conversion into $C_xF_{2x+1}O_2$ radicals followed by reaction with CH_3O_2 radicals to give an alcohol which undergoes heterogeneous elimination of HF to give an acyl fluoride which then reacts with water

$$C_xF_{2x+1}CHO + h\nu \rightarrow C_xF_{2x+1} + HCO$$

$$C_xF_{2x+1} + O_2 + M \rightarrow C_xF_{2x+1}O_2 + M$$

$$C_xF_{2x+1}O_2 + CH_3O_2 \rightarrow C_xF_{2x+1}OH + HCHO + O_2$$

$$C_xF_{2x+1}OH \rightarrow C_{x-1}F_{2x-1}C(O)F + HF$$

$$C_{x-1}F_{2x-1}C(O)F + H_2O \rightarrow C_{x-1}F_{2x-1}C(O)OH + HF$$

The relative importance of these two mechanisms depends on many factors, not least of which being the relative importance of the reaction with OH and photolysis as loss mechanisms for $C_xF_{2x+1}CHO$. The new finding in the present work that photolysis is the dominant atmospheric fate of $C_xF_{2x+1}CHO$ ($x = 1-4$) suggests that the first mechanism outlined above is less important than previously thought. The photolysis of perfluoroaldehydes ($C_xF_{2x+1}CHO$) and fluorotelomer aldehydes ($C_xF_{2x+1}CH_2CHO$) needs to be included in future atmospheric models to assess the perfluorocarboxylic acid yield during the atmospheric oxidation of fluorotelomer alcohols.

Acknowledgment. M.S.C., F.E.M., and G.A.A. thank E.I. duPont de Nemours for a grant to conduct this work.

Supporting Information Available: UV−vis spectra of aldehydes at different temperatures and 1 nm spaced absorption cross sections are listed in Figures S1−5 and the table, respectively. This material is available free of charge via the Internet at http://pubs.acs.org.

References and Notes

(1) Calafat, A. M.; Kuklenyik, Z; Caudill, S. P.; Reidy, J. A.; Needham, L. L. *Environ. Sci.* Technol. **2006**, *40*, 2128.

(2) Smithwick, M.; Norstrom, R. J.; Mabury, S. A.; Solomon, K.; Evans, T. J.; Stirling, I.; Taylor, M. K.; Muir, D. C. G. *Environ. Sci.* Technol. **2006**, *40*, 1139.

(3) Yamashita, N.; Kannan, K.; Taniyasu, S.; Horii, Y.; Petrick, G.; Gamo, T. *Mar. Pollut. Bull.* **2005**, *51*, 658.

(4) Yeung, L. W. Y.; So, M. K.; Jiang, G.; Taniyasu, S.; Yamashita, N.; Song, M.; Wu, Y.; Li, J.; Giesy, J. P.; Guruge, K. S.; Lam, P. K. S. *Environ. Sci.* Technol. **2006**, *40*, 715.

(5) 3M Company. *Fluorochemical Use, Distribution and Release Overview*; U. S. EPA Administrative Record AR226−0550; U. S. Environmental Protection Agency; U. S. Government Printing Office: Washington, DC, 1999.

(6) Prevedouros, K.; Cousins, I. T; Buck, R. C.; Korzeniowski, S. H. *Environ.* Sci. Technol. **2006**, *40*, 32.

(7) Stock, N. L.; Lau, F. K.; Ellis, D. A.; Martin, J. W.; Muir, D. C. G.; Mabury, S. A. *Environ.* Sci. Technol. **2004**, *38*, 991.

(8) Martin, J. W.; Muir, D. C. G.; Moody, C. A.; Ellis, D. A.; Kwan, W. C.; Solomon, K. R.; Mabury, S. A. *Anal. Chem.* **2002**, *74*, 584.

(9) Shoeib, M.; Harner, T.; Ikonomou, M.; Kannan, K. *Environ.* Sci. Technol. **2004**, *38*, 1313.

(10) Shoeib, M.; Harner, T.; Wilford, B. H.; Jones, K. C.; Zhu, J. *Environ.* Sci. Technol. **2005**, *39*, 6599.

(11) D'Eon, J. C.; Hurley, M. D.; Wallington, T. J.; Mabury, S. A. *Environ. Sci. Technol.* **2006**, *40*, 1862.

(12) Martin, J. W.; Ellis, D. A.; Mabury, S. A.; Hurley, M. D.; Wallington, T. J. *Environ. Sci. Technol.* **2006**, *40*, 864.

(13) Ellis, D. A.; Martin, J. W.; De Silva, A. O.; Mabury, S. A.; Hurley, M. D.; Sulbaek Andersen, M. P.; Wallington, T. J. *Environ. Sci. Technol.* **2004**, *38*, 3316.

(14) Wang, N.; Szostek, B.; Buck, R. C.; Folsom, P. W.; Sulecki, L. M.; Capka, V.; Berti, W. R.; Gannon, J. T. *Environ. Sci. Technol.* **2005**, *39*, 7516.

(15) Wang, N.; Szostek, B.; Folsom, P. W.; Sulecki, L. M.; Capka, V.; Buck, R. C.; Berti, W. R.; Gannon, J. T. *Environ. Sci. Technol.* **2005**, *39*, 531.

(16) Li, Y.; Demerjian, K.; Williams, L.; Worsnop, D.; Kolb, C.; Davidovits, P. *J. Phys.* Chem. *A* **2006**, *110*, 6814.

(17) Goss, K.; Bronner, G.; Harner, T.; Hertel, M.; Schmidt, T. *Environ. Sci. Technol.* **2006**, *40*, 3572.

(18) Frank, H.; Christoph, E. H.; Holm-Hansen, O.; Bullister, J. L. *Environ. Sci. Technol.* **2002**, *36*, 12.

(19) Wallington, T. J.; Hurley, M. D.; Xia, J.; Wuebbles, D. J.; Sillman, S.; Ito, A.; Penner, J. E.; Ellis, D. A.; Martin, J.; Mabury, S. A.; Nielsen, O. J.; Sulbaek Andersen, M. P. *Environ. Sci. Technol*. **2006**, *40*, 924.

(20) Sellevåg, S. R.; Stenstrom, Y.; Helgaker, T.; Nielsen, C. J. *J. Phys. Chem. A* **2005**, *109*, 3652.

(21) Sellevåg, S. R.; Kelly, T.; Sidebottom, H.; Nielsen, C. J. *Phys. Chem. Chem. Phys*. **2004**, *6*, 1243.

(22) Rattigan, O. V.; Wild, O.; Cox, R. A. *J. Photochem. Photobiol., A* **1998**, *112*, 1.

(23) Meller, R.; Moortgat, G. K. *J. Geophys. Res., [Atmospheres]* **2000**, *105*, 7089.

(24) Malanca, F. E.; Chiappero, M. S.; Wallington, T. J.; Argüello, G. A. *Atmos. Environ*. **2005**, *39*, 5051.

(25) Malanca, F. E.; Chiappero, M. S.; Argüello, G. A. *J. Photochem. Photobiol., A* **2006**, in press, corrected proof, available online 28 April 2006; doi: 10.1016/j.jphotochem.2006.08.019.

(26) Sulbaek Andersen, M. P.; Hurley, M. D.; Wallington, T. J.; Ball, J. C.; Martin, J. W.; Ellis, D. A.; Mabury, S. A.; Nielsen, O. J. *Chem. Phys. Lett*. **2003**, *379*, 28.

(27) Chamberlain, G. A.; Whittle, E. *Trans. Faraday Soc.* **1971**, 88.

(28) Atkinson, R.; Baulch, D. L.; Cox, R. A.; Crowley, J. N.; Hampson, R. F., Jr.; Kerr, J.A.; Rossi, M. J.; Troe, J. *Summary of Evaluated Kinetics and Photochemical Data for Atmospheric Chemistry*; IUPAC Subcommittee on Gas Kinetics Data Evaluation for Atmospheric Chemistry; Web version 2006; http://www.iupac-kinetic.ch.cam.ac.uk/.

(29) Borkowski, R. P.; Ausloss, P. *J. Am. Chem. Soc.* **1962**, *84*, 4044.

(30) Lucazeau, G.; Sandorfy, C. *J. Mol. Spectrosc.* **1970**, *35*, 214.

(31) Francisco, J. S.; Williams, I. H. *Mol. Phys.* **1992**, *6*, 1433.

(32) Meller, R.; Boglu, D.; Moortgat, G. K. In *STEP*−HALOCSIDE/AFEAS Workshop; Dublin, Ireland, March 23−25, 1993; pp 130−138.
(33) Hashikawa, Y.; Kawasaki, M.; Waterland, R. L.; Sulbaek Andersen, M. P.; Nielsen, O. J.; Hurley, M. D.; Ball, J. C.; Wallington, T. J. *J. Fluorine Chem.* **2004**, *125*, 1925.
(34) Pritchard, G. O.; Miller, G. H.; Foote, J. K. *Can. J. Chem.* **1962**, *40*, 1830.
(35) Madronich, S., Flocke, S. In *Handbook of Environmental Chemistry*; Boule, P., Ed.; Springer: Heidelberg, 1998; pp 1−26.
(36) Sulbaek Andersen, M. P.; Toft, A.; Nielsen, O. J.; Hurley, M. D.; Wallington, T. J.; Chishima, H.; Tonokura, K.; Mabury, S. A.; Martin, J. W.; Ellis, D. A. *J. Phys. Chem. A* **2006**, *110*, 9854.
(37) Wallington, T. J.; Schneider, W. F.; Worsnop, D. R.; Nielsen, O. J.; Sehested, J.; DeBruyn, W.; Shorter, J. A. *Environ. Sci. Technol.* **1994**, *28*, 320A.
(38) DeBruyn, W. J.; Shorter, J. A.; Davidovits, P.; Worsnop, D. R.; Zahniser, M. S.; Kolb, C. E. *Environ. Sci. Technol.* **1995**, *29*, 1179.
(39) Morris, E. R.; Thynne, J. C. J. *J. Phys. Chem.* **1968**, *72*, 3351.
(40) Dodd, R. E.; Smith, J. W. *J. Chem. Soc.* **1957**, 1465; doi: 10.1039/JR9570001465.
(41) Pearce, C.; Whytock, D. A. *J. Chem. Soc., Chem. Commun.* **1971**, 1464; doi: 10.1039/C29710001464.
(42) Richter, H. R.; Sodeau, J. R.; Barnes, I. In *STEP*−HALOCSIDE/AFEAS Workshop; Dublin, March 23−25, 1993; pp 130−138.